catalysts

MDPI

Article

Effect of the Gallium and Vanadium on the Dibenzothiophene Hydrodesulfurization and Naphthalene Hydrogenation Activities Using Sulfided NiMo-V_2O_5/Al_2O_3-Ga_2O_3

Esneyder Puello-Polo [1], Yina Pájaro [2] and Edgar Márquez [3,*]

1 Grupo de Investigación en Oxi/Hidrotratamiento Catalítico y Nuevos Materiales, Programa de Química-Ciencias Básicas Universidad del Atlántico, Puerto Colombia 081001, Colombia; esneyderpuello@mail.uniatlantico.edu.co

2 Grupo de Investigación en Farmacia Asistencial y Farmacología (GIFAF), Facultad de Química y Farmacia Universidad del Atlántico, Puerto Colombia 081001, Colombia; yinapagon@yahoo.es

3 Grupo de Investigación en Química y Biología, Departamento de Química y Biología, Universidad del Norte, Barranquilla 081007, Colombia

* Correspondence: ebrazon@uninorte.edu.co

Received: 4 July 2020; Accepted: 27 July 2020; Published: 7 August 2020

Abstract: The effect of Ga and V as support-modifier and promoter of NiMoV/Al2O3-Ga2O3 catalyst on hydrogenation (HYD) and hydrodesulfurization (HDS) activities was studied. The catalysts were characterized by elemental analysis, textural properties, XRD, XPS, EDS elemental mapping and High-resolution transmission electron microscopy (HRTEM). The chemical analyses by X-ray Fluorescence (XRF) and CHNS-O elemental analysis showed results for all compounds in agreement, within experimental accuracy, according to stoichiometric values proposed to Mo/Ni = 6 and (V+Ni)/(V+Ni+Mo) = 0.35. The sol-gel synthesis method increased the surface area by incorporation of Ga^{3+} ions into the Al_2O_3 forming Ga-O-Al bonding; whereas the impregnation synthesis method leads to decrease by blocking of alumina pores, as follows NiMoV/Al-Ga(1%-I) < NiMoV/Al-Ga(1%-SG) < NiMo/Al_2O_3 < Al_2O_3-Ga_2O_3(1%-I) < Al_2O_3-Ga_2O_3(1%-SG) < Al_2O_3, propitiating Dp-BJH between 6.18 and 7.89 nm. XRD confirmed a bulk structure typical of $(NH_4)_{4[}NiMo_6O_{24}H_6]\bullet 5H_2O$ and XPS the presence at the surface of Mo^{4+}, Mo^{6+}, NixSy, Ni^{2+}, Ga^{3+} and V^{5+} species, respectively. The EDS elemental mapping confirmed that Ni, Mo, Al, Ga, V and S are well-distributed on Al_2O_3-Ga_2O_3(1%-SG) support. The HRTEM analysis shows that the length and stacking distribution of MoS_2 crystallites varied from 5.07 to 5.94 nm and 2.74 to 3.58 with synthesis method (SG to I). The results of the characterization sulfided catalysts showed that the synthesis method via impregnation induced largest presence of gallium on the surface influencing the dispersion V^{5+} species, this effect improves the dispersion of the MoS_2 phase and increasing the number of active sites, which correlates well with the dibenzothiophene HDS and naphthalene HYD activities. The dibenzothiophene HDS activities with overall pseudo-first-order rate constants' values (k_{HDS}) from 1.65 to 7.07 L/(h·mol·m^2) follow the order: NiMoV-S/Al-Ga(1%-I) < NiMo-S/Al_2O_3 < NiMoV-S/Al-Ga(1%-SG), whereas the rate constants' values (k) of naphthalene HYD from 0.022 to 2.23 L/(h·mol·m^2) as follow: NiMoV-S/Al-Ga(1%-SG) < NiMo-S/Al_2O_3 < NiMoV-S/Al-Ga(1%-I). We consider that Ga and V act as structural promoters in the NiMo catalysts supported on Al_2O_3 that allows the largest generation of BRIM sites for HYD and CUS sites for DDS.

Keywords: gallium; vanadium; hydrodesulfurization; hydrogenation; synthesis method

1. Introduction

The hydrotreating processes (HDT) uses hydrogenolysis and hydrogenation reactions to remove contaminants such as sulfur, nitrogen, oxygen and metals, and saturate hydrocarbons from liquid petroleum fractions within an oil refinery [1,2]. Catalytic hydrotreating depends largely on the origin of the feed, the operating conditions and the nature of the catalyst with the purpose of increase the quality of transportation fuels [3]. The current generation of hydrotreating catalysts are alumina supported Ni(Co) promoted Mo(W) sulfides; however, these catalysts have some defects, such as the difficulty in its sulfurization and the strong interaction between support and active species [4]. In these catalysts, the models by Topsøe and Chianelli propose that the active sites in these reactions are attributed to sites located on the edges, corners, BRIM or RIM [5,6]. The new regulations nowadays which aim at a severe oil feedstock specifications represent a challenging task for oil refineries [7]. In Colombia, the Ministries of Mines and Energy, in 2014 issued regulations that lead to improved quality of diesel in terms of sulfur and polycyclic aromatic content[8]. To achieve these regulations, in the last decades, efforts have been tried to improve the catalytic properties of traditional catalysts, such as changing the active phase and promoter, varying the preparation method and modifying the support [9,10]. In this sense, many studies describe the influence of support on the performance of HDT catalysts, because their interaction with the active phase determines the morphology, dispersion, sulfur lability, mobility and stability of the corresponding metal site [11]. Usually, the alumina is the catalytic support most used HDT, since it has excellent mechanical, low cost and ability to provide dispersion properties [12]. However, the active components are loaded on it through an impregnation method, which leads to a calcination step that causes the formation of Ni(Co)Mo(W)-AlO_4 species (compounds not active in HDT). Hence, recent studies have shown use alumina-modifier elements such as boron, fluorine, phosphorus, silicon, zeolites [13,14], magnesium [15], titanium [16], zinc [17], which could increase the dispersion of the active phase and decrease the active phase(promoter)–support interactions. By taking into account of these limitations, recent studies have shown as potential active phase for such applications the Anderson type polyoxomolybdates [18]. The planar structure of the Anderson type polyoxomolybdates is a relevant factor, producing an active surface with an ordered distribution and uniform deposition, besides the suppression of calcination steps during the activation process could avoid the decrease of active Ni(Co) which favors the synergic effect, doing it an interesting alternative to HDS traditional systems [19].

The addition of gallium and vanadium for the preparation NiMo/Al catalysts has been reported by De los Reyes, who suggested that the Ga^{3+} added to alumina increased HDS activity [20,21]. Cimino and Lo Jacono reported the modification of Ni tetrahedral/octahedral ratio in Ni/Al_2O_3 catalysts by the addition of Ga^{3+} to alumina [22]. Zepeda et al. demonstrated that the addition of Ga has a strong effect on the CUS, improving the HYD mechanism in the HDS reaction [23]. Petre et al. found that the acidity of the support was modified with Ga, increasing its HDS activity and modifying the desulfurization (DDS)/HYD selectivity [24]. Altamirano et al. reported that the addition of Ga inhibit the formation of Ni(Co)Al_2O_4 and it improves the sulfiding of the active species [20].

On the other hand, studies have shown that small amounts of vanadium to hydrotreating catalyst leads to the increase in the support acidity as reported by De Jonghe et al. in his study on toluene HYD using V-NiMo catalysts [25]. In this sense, Rankell and Rollman showed that VSx was active for HDT [26]. Lacroix [27] prepared VSx and it was more active in HDS than that MoS_2 and WS_2, respectively. Paulino et al. have obtained V-based catalysts promoting the HDS and HDN of LCO (7 times greater activities than MoS_2) [28,29]. Escalante et al. showed that Al-MCM-41-supported V sulfides catalysts presented the highest formation of hydrogenated products in the thiophene HDS due to the support nature with lower Si/Al(Zr) ratios [30].

In this regard, seeing the importance of Ga and V separately to hydrotreating reactions the present work reports the effect of the addition of Ga and V in NiMoV/Al_2O_3-Ga_2O_3 catalyst by two different preparation methods looking to enhance their desulfurization and hydrogenating properties on the HDS and HYD activity of dibenzothiophene and naphthalene.

2. Results and Discussion

2.1. Chemical Analysis

Table 1 shows the experimental chemical analyses of Al_2O_3-Ga_2O_3(1%-SG), Al_2O_3-Ga_2O_3(1%-I), NiMo/Al_2O_3, NiMoV/Al-Ga(1%-SG) and NiMoV/Al-Ga(1%-I) by XRF. The relative deviations between experimental and theoretical could relate to the synthesis procedures. Nevertheless, the experimental accuracy of Mo/Ni and (V+Ni)/(V+Ni+Mo) are in agree with the composition nominal proposed, i.e., 6 and 0.35, respectively [31].

Table 1. Experimental Composition (wt%) and textural properties of supports and NiMoV/Al-Ga(1%-x) catalyst varying the synthesis method (x= SG and I).

Solid	Experimental Composition (wt%)-XRF						Textural Properties				
	Mo	Ni	Ga_2O_3	V_2O_5	$\frac{V+Ni}{Mo+V+Ni}$	$\frac{Mo}{Ni}$	S_{BET}	S_{ext} (m^2/g)	S_{micro}	V_p (cm^3/g)	D_p (nm)
Al_2O_3							265	258	7	0.57	7.68
Al_2O_3-Ga_2O_3(1%-SG)			1.46				259			0.52	6.97
Al_2O_3-Ga_2O_3(1%-I)			1.51				238			0.45	6.78
NiMo/Al_2O_3	25.02	2.38				6.5	233	184	49	0.26	7.20
NiMoV/Al-Ga(1%-SG)	24.02	2.38	0.99	6.43	0.31	6.2	172	160	12	0.37	7.89
NiMoV/Al-Ga(1%-I)	25.60	2.47	0.94	6.57	0.30	6.3	139	138	1	0.23	6.18

SG: sol-gel synthesis; I: impregnation synthesis; S_{BET}: BET surface area; S_{micro}: micropores surface area; S_{ext}: external surface area; Composition Nominal: 20 wt% Mo, 2.04 wt%, 5.5 wt% V_2O_5, 1 wt% Ga_2O_3; (V + Ni)/(Mo + V + Ni) = 0.35, Ni/Mo = 6.

2.2. Textural Properties

All the N_2 physisorption isotherms shown in Figure 1 are type IV in the IUPAC classification [32]. The hysteresis loops showed that Al_2O_3 is type H1 due to uniform mesopores and, Al_2O_3-Ga_2O_3(1%-SG), Al_2O_3-Ga_2O_3(1%-I) and NiMoV/Al-Ga(1%-SG) types a combination of H1 and H2 related to the ink-bottle and uniform type of mesopores, respectively; while NiMoV/Al-Ga(1%-I) displayed a combination of H2 and H3 due to ink-bottle and laminar type mesopores. The isotherms behavior demonstrates the influence of the synthesis method on textural properties of the catalysts [32].

The Table 1 shows that the textural characteristics of the supports and catalysts using supports obtained by the sol-gel synthesis method are greater than those obtained by the conventional impregnation method due to the migration of the metallic phase (Ni, Mo, Ga and V) into the support pores during the impregnation process and/or synthesis of the material that decreases their pore volume and therefore the surface area [33]. Hence, the overall surface area was found to increase as follows: NiMoV/Al-Ga(1%-I) < NiMoV/Al-Ga(1%-SG) < NiMo/Al_2O_3 < Al_2O_3-Ga_2O_3(1%-I) < Al_2O_3-Ga_2O_3(1%-SG) < Al_2O_3; whereas the pore volume showed to increase as follows: NiMoV/Al-Ga(1%-I) < NiMo/Al_2O_3 < NiMoV/Al-Ga(1%-SG) < Al_2O_3-Ga_2O_3(1%-I) < Al_2O_3-Ga_2O_3(1%-SG) < Al_2O_3. The comparison of the supports shows an increase in the surface area and pore volume with the variation of the synthesis method, which means that the Ga^{3+} ions are incorporated into the Al_2O_3 structure (Ga^{3+} ion > Al^{3+} ion) [34,35].

Thus, when comparing the Al_2O_3 with NiMo/Al_2O_3, NiMoV/Al-Ga(1%-SG) and NiMoV/Al-Ga(1%-I) was observed that the S_{micro}/S_{BET} varies between 0.72 and 26.6 %, which can be attributed to the generation of microporosity induced by the migration of the metallic phase, although it decreases with the presence of Ga and V[36]. All the pore size distribution was unimodal (see Table 1 and Figure 1) with pore diameters located in the range of mesoporous (2–50 nm) [32], with values of BJH mesopores mean size between 6.18 and 7.89 nm in the order: NiMoV/Al-Ga(1%-I) < Al_2O_3-Ga_2O_3(1%-I) < Al_2O_3-Ga_2O_3(1%-SG) < NiMo/Al_2O_3 < Al_2O_3 < NiMoV/Al-Ga(1%-SG) [33].

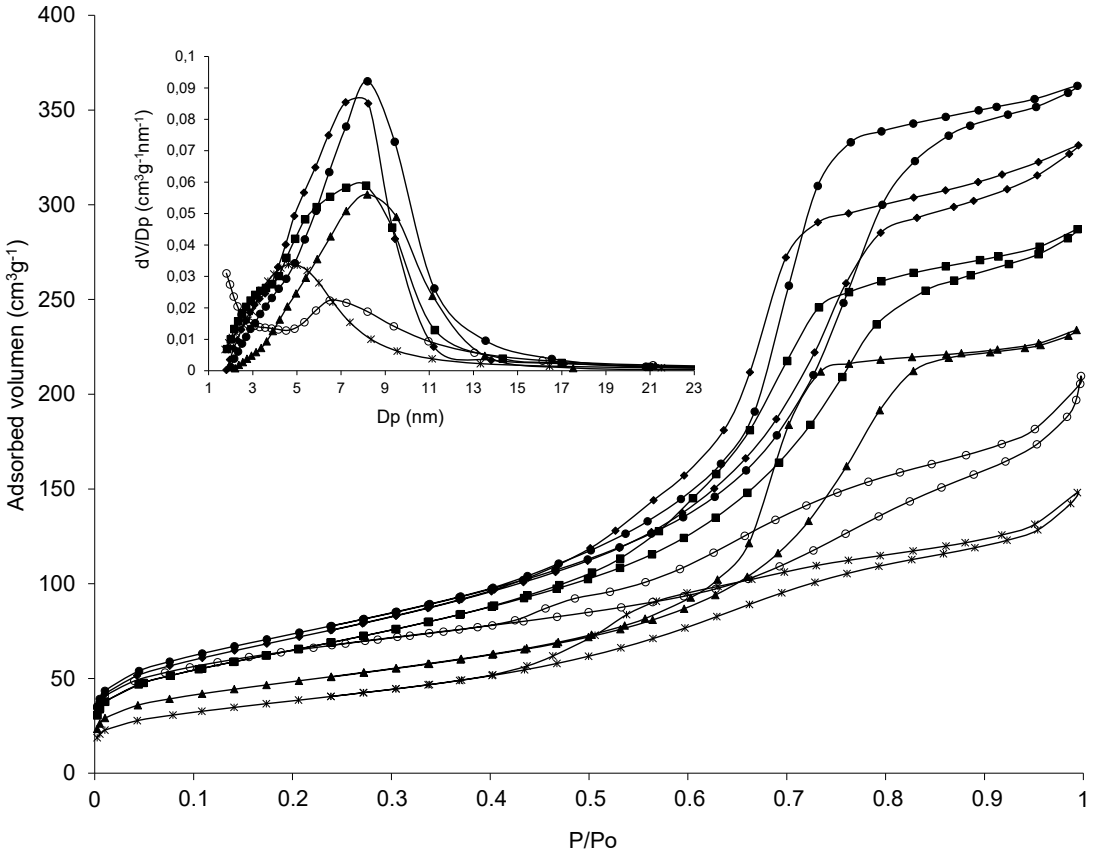

Figure 1. Adsorption/desorption isotherms of N_2 at 77 K and pore size distribution of the supports and NiMoV/Al-Ga(1%-x) catalyst varying the synthesis method (x = SG and I). (●) Al_2O_3; (♦) Al_2O_3-Ga_2O_3(1%-SG); (■) Al_2O_3-Ga_2O_3(1%-I); (○) NiMo/Al_2O_3; (▲) NiMoV/Al-Ga(1%-SG); (ж) NiMoV/Al-Ga(1%-I).

2.3. XRD Analysis

The XRD patterns of oxidic precursors corresponding to Al_2O_3 or Al_2O_3-Ga_2O_3 supported $(NH_4)_4[NiMo_6O_{24}H_6]\bullet 5H_2O$ are shown in Figure 2 [37]. In this figure and regardless of the synthesis method of the support, all the precursors revealed no lines other than those corresponding to $(NH_4)_4[NiMo_6O_{24}H_6]\bullet 5H_2O$ (JCPDS 52-0167) at 2θ = 11.191(100), 15.211($10\bar{1}$), 16.402(020), 17.548($11\bar{1}$), 23.772($20\bar{1}$), 28.587(031), 29.555(211) and γ-Al_2O_3 (JCPDS 10-0425) at 2θ = 67.034(440), 60.899(511), 45.863(400), 39.492(222), 37.604(311), 31.937(220), 19.451(111). The diffraction peaks corresponding to $(NH_4)_4[NiMo_6O_{24}H_6]\bullet 5H_2O$ are narrow, intense and defined, suggesting high crystallinity with greater effect in NiMoV/Al-Ga(1%-SG). Likewise, the XRD pattern of Al_2O_3-Ga_2O_3(1%-SG) and Al_2O_3-Ga_2O_3(1%-SG) shows that the presence of Ga causes a better crystallinity of the Al_2O_3, but a slight shift of diffraction peaks toward larger angles, suggesting a decrease in the interplanar distance which may be related to the changes in porosity in the materials and likewise the precursors. On the other hand, Figure 2, revealed no diffraction lines due to γ-Ga_2O_3 (JCPDS 020-0426, 2θ = 36.191, 64.179) and V_2O_5 (JCPDS 010-0359, 2θ = 20.258, 26.268, 31.138) probably because were well dispersed on the support and/or the crystallites are too small to give XRD signals [31].

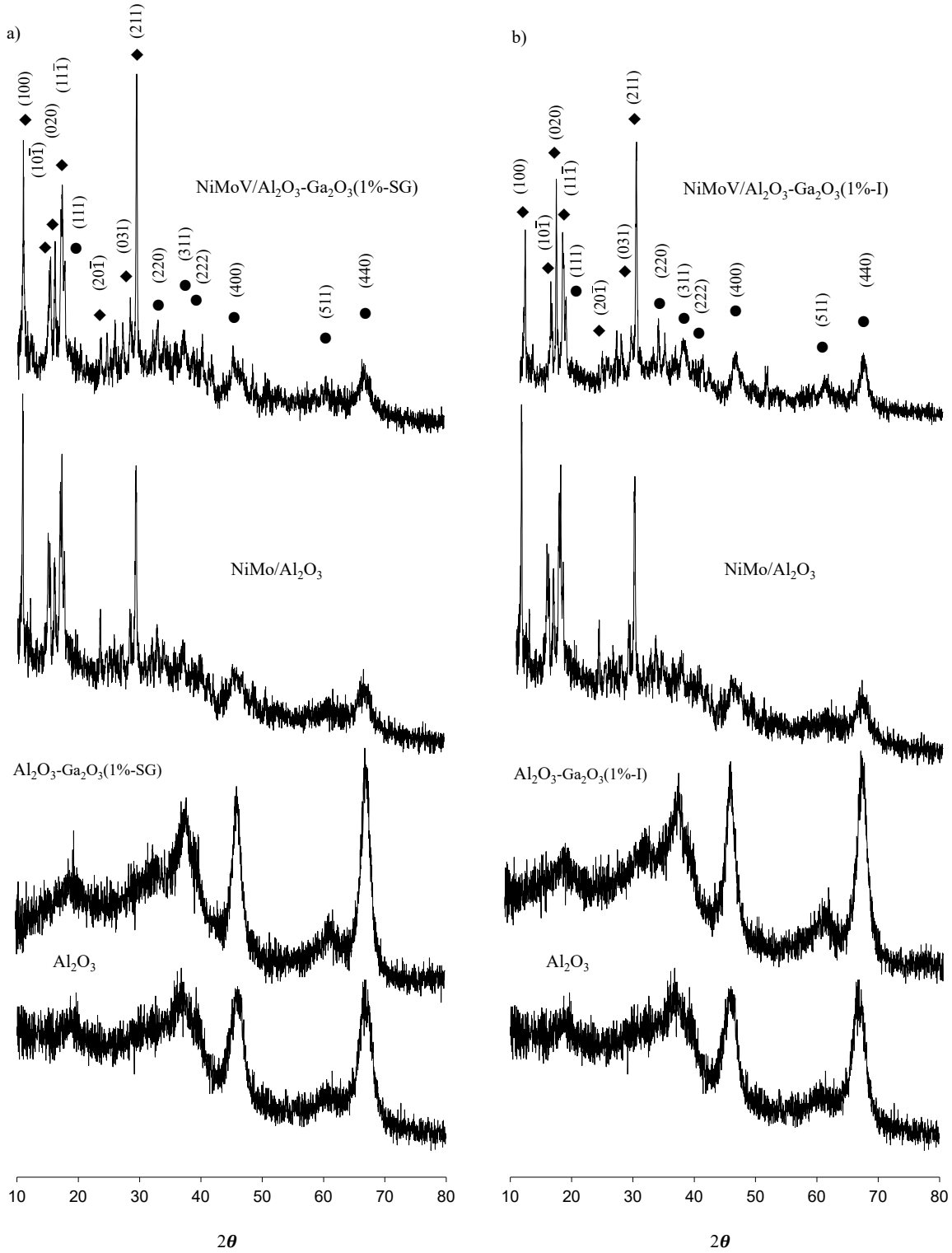

Figure 2. X-ray diffraction patterns of supports and NiMoV/Al-Ga(1%-x) catalyst varying the synthesis method (x = SG and I): (**a**) sol-gel synthesis and (**b**) impregnation synthesis. (•) Al_2O_3; (♦) $(NH_4)_4[NiMo_6O_{24}H_6]•5H_2O$.

2.4. XPS Analysis

The Figure 2 shows XPS analysis of NiMoV-S/Al-Ga(1%-x). XPS region of Mo $3d_{5/2\text{-}3/2}$ showed signals on the surface of Mo^{4+} (229 eV), Mo^{6+} (232.5 eV) and 2s (226.5 eV), which might be attributable

to the Mo sulfide phase, MoO_3 and signal of sulfur [38–40]. The higher amount of Mo^{4+} species using the synthesis method of impregnation, suggesting that the increased presence on the surface of gallium and vanadium by impregnation method has a positive effect on reducibility (see Figure 3I). The signal of sulfur in the Mo $3d_{5/2\text{-}3/2}$ region can be confirmed by the presence of three bands in the S $2p_{3/2}$ region [39]: a signal at 161.7 eV due to terminal disulfide and/or sulfide (S^{2-}), another signal at 163.1 eV corresponding to bridging disulfide (S_2^{2-}) ligands and the signal at 168.9 eV, which can be assigned to SO_4^{2-} (see Figure 3III). The signals due to sulfide species are much more important for the catalyst with support modified by impregnation, which showed no presence of sulfates (see Table 2).

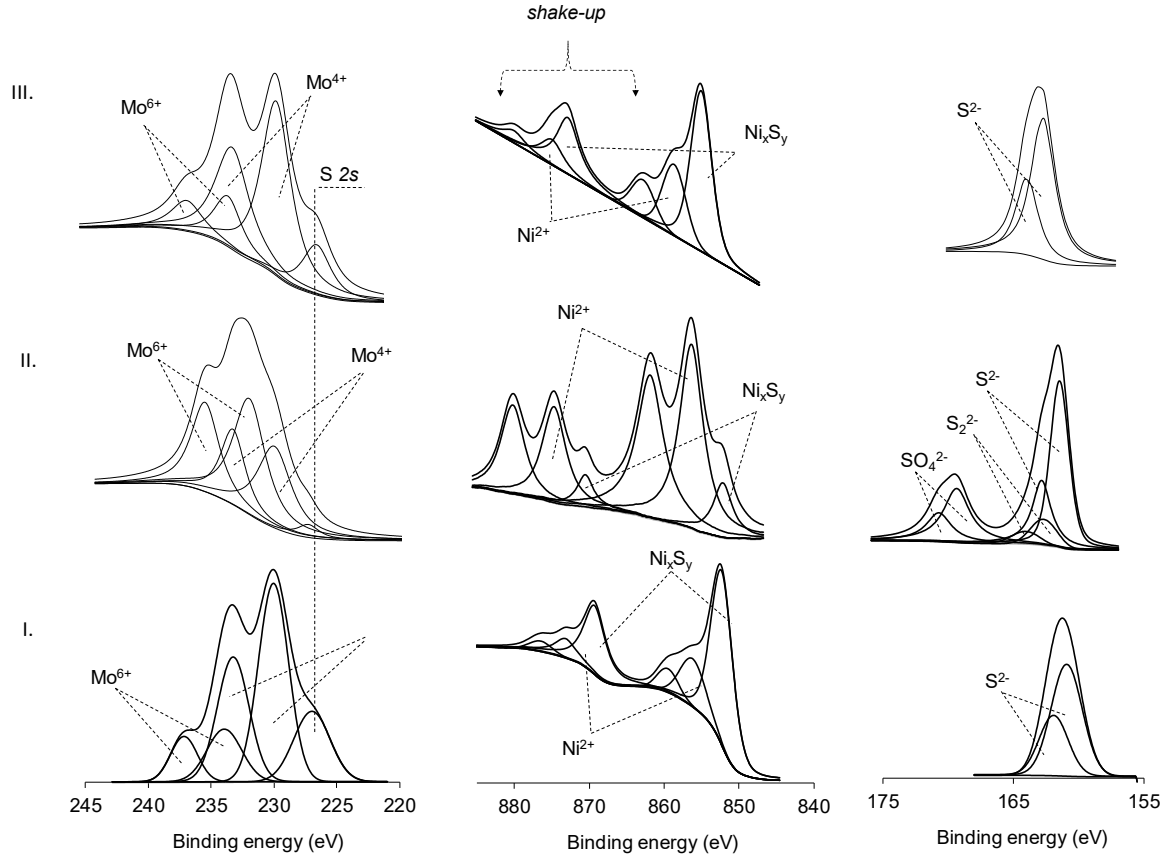

Figure 3. X-ray photoelectron spectra Mo 3d, Ni 2p and S 2p regions of sulfided NiMoV/Al-Ga(1%-x) catalyst varying the synthesis method (x = SG and I): (**I**) NiMo-S/Al_2O_3; (**II**) NiMoV-S/Al-Ga(1%-SG); (**III**) NiMoV-S/Al-Ga(1%-I).

Meanwhile, the Ni 2p region spectra of Figure 3II shows three Ni $2p_{3/2\text{-}1/2}$ peaks at 853.1–853.6; 856.1–856.7 and 862 eV [41,42]. These signals suggest, respectively, the presence of NixSy sulfide phases (Ni_2S_3, Ni_9S_8 or NiS), the $NiMoO_4$ species, and the strong shake-up lines characteristic of Ni^{2+} species in a Ni-Mo-O matrix. Note that the signal of Ni does not show considerable variation in the type of Ni species on surface independently of the support synthesis method, although the proportion of Ni is greater in the impregnation synthesis method (see Table 2). The XPS spectra in the Ga 3d and V $2p_{3/2\text{-}1/2}$ regions (not shown here), the Ga^{3+} (20.5 eV) and V^{5+} (517.1 eV) signals could be attributable to Ga_2O_3 and V_2O_5 with amounts from 0.1 to 0.6 on the surface [43,44].

Table 2. Distribution of Mo, Ni, S, Ga and V oxidation states by XPS and morphology of the MoS_2 active phase determined by HRTEM in sulfided NiMoV-S/Al-Ga(1%-x) catalyst varying the synthesis method (x = SG and I).

Catalyst	Mo $3d_{5/2}$-$3d_{3/2}$		Ni $2p_{3/2}$-$2p_{1/2}$		S $2p_{3/2}$-$2p_{1/2}$			MoS_2 Characteristics		
	Mo^{4+} 229 eV (%)	Mo^{6+} 232.5 eV (%)	Ni_xS_y 853.3 eV (%)	$NiMoO_4$ 856.1 eV (%)	S^{2-} 161.7 eV (%)	S_2^{2-} 163.1 eV (%)	SO_4^{2-} 168.9 eV (%)	L (nm)	N	$(fe/fc)_{Mo}$
$NiMo-S/Al_2O_3$	3.30	1.00	0.46	0.14	6.50					
NiMoV-S/Al-Ga(1%-SG)	2.08	2.82	0.083	0.22	1.09	0.22	0.65	5.07	2.74	6.43
NiMoV-S/Al-Ga(1%-I)	2.13	0.57	0.42	0.18	3.60			5.94	3.58	7.79

L (average length) and N (average stacking degree) of MoS_2 crystallites; $(fe/fc)_{Mo}$: estimated fraction of Mo atoms on the edge surface of MoS_2 particles.

The previous experimental results may be due to the presence of different V^{5+} species on surface, that is, when the support is modified with Ga, small V rich-aggregates on the surface could predominate depending on their dispersion associated to the solubility of the precursors during synthesis [30]. In the synthesis method by impregnation is possible that, in the Al_2O_3-Ga_2O_3(1%-I) support, a large number of Ga^{3+} sites will be available on the surface even after impregnating the V, which is reflected in the good reducing and sulfiding of the Anderson type polyoxomolybdates as seen in the NiMoV-S/Al-Ga(1%-I) catalysts. While in Al_2O_3-Ga_2O_3(1%-SG) there a greater dispersion of the V species.

2.5. SEM Analysis with Energy Dispersive X-ray Spectroscopy and Elemental Mapping

The SEM microscopy of the NiMoV-S/Al-Ga(1%-SG) and NiMoV-S/Al-Ga(1%-I) catalysts showed that the morphologies consist of particle cumulus with irregular geometries, being smaller particles for NiMoV-S/Al-Ga(1%-SG) as displayed the Figure 4. The EDS elemental mapping confirmed the presence of the atoms constituting the catalysts, i.e., Mo, Ni, Al, O, Ga, V and S. These elements are well-distributed on the support as shown by EDS elemental mapping (Figures 4 and 5). However, the Mo, V and S atoms in NiMoV-S/Al-Ga(1%-I) could not disperse in the whole selected area, suggesting that the concentration of these elements is slightly larger in few catalyst zones ("cluster"), hence the differences observed for V can be associated to the solubility of the precursors, suggesting that some V atoms could precipitate on the support surface forming V rich-aggregates [45].

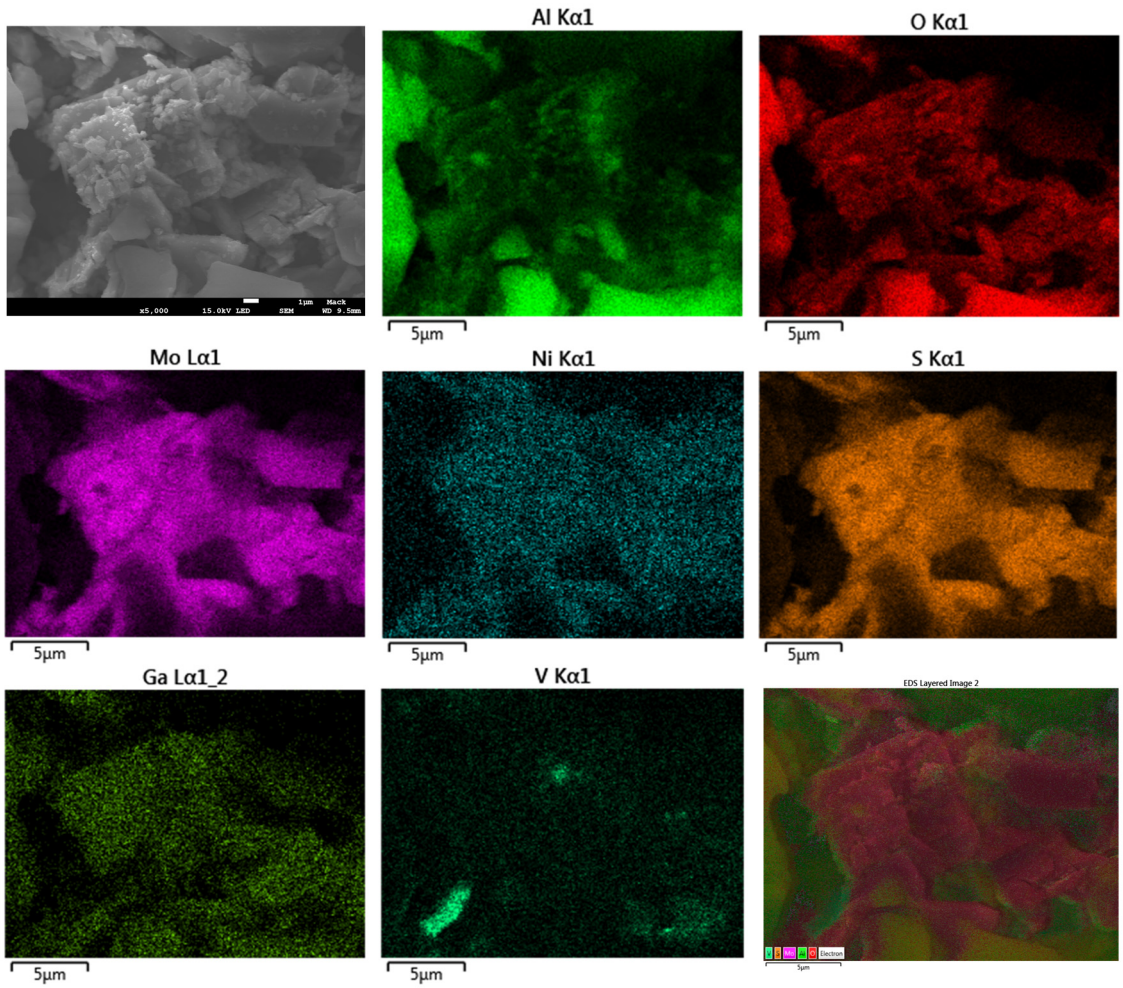

Figure 4. EDS elemental mapping of Mo, Ni, S, Ga, V, Al and O in NiMoV-S/Al-Ga(1%-SG).

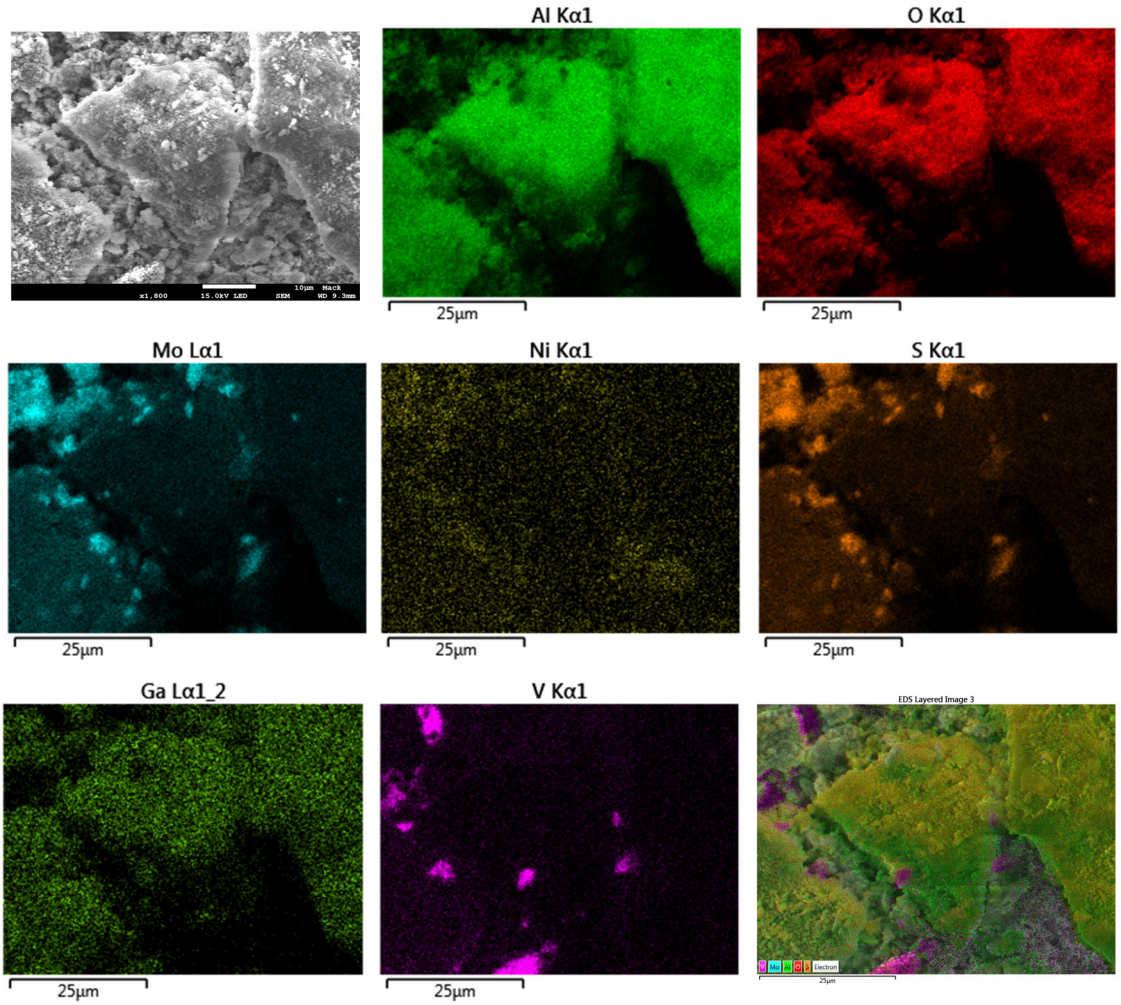

Figure 5. EDS elemental mapping of Mo, Ni, S, Ga, V, Al and O in sulfided NiMoV-S/Al-Ga(1%-I).

2.6. High-Resolution Transmission Electron Microscopy

The HRTEM analysis for NiMoV-S/Al-Ga(1%-SG) and NiMoV-S/Al-Ga(1%-I) is shown in the Figures 6 and 7. The HRTEM micrographs display the presence of homogeneously dispersed MoS_2 crystallites with multi-layers (black thread-like fringes with separation of 0.65 nm characteristic of the basal planes (002)), whose values of D showed higher dispersion of the catalytically active MoS_2 phase in NiMoV-S/Al-Ga(1%-SG) than NiMoV-S/Al-Ga(1%-I) (see Table 2). The Figures 6 and 7 shows that the length and stacking distribution of MoS_2 crystallites changes with the support synthesis method (SG vs. I), which varied from 5.07 to 5.94 nm and 2.74 to 3.58, respectively [46]. Thus, HRTEM image shows that the impregnation method led to the agglomeration of Ni, Mo and V, which was confirmed with the increase in the length and stacking number of the NiMoS phase. This conclusion was also corroborated by EDS elemental mapping (Figure 5). While for the catalyst obtained via sol-gel was improved the dispersion of NiMo species (D = 0.19 vs. 0.20). Meanwhile, the edge-to-corner ratio a MoS_2 slab $(fe/fc)_{Mo}$ increased as the average slab length increased (6.43 to 7.79) [46].

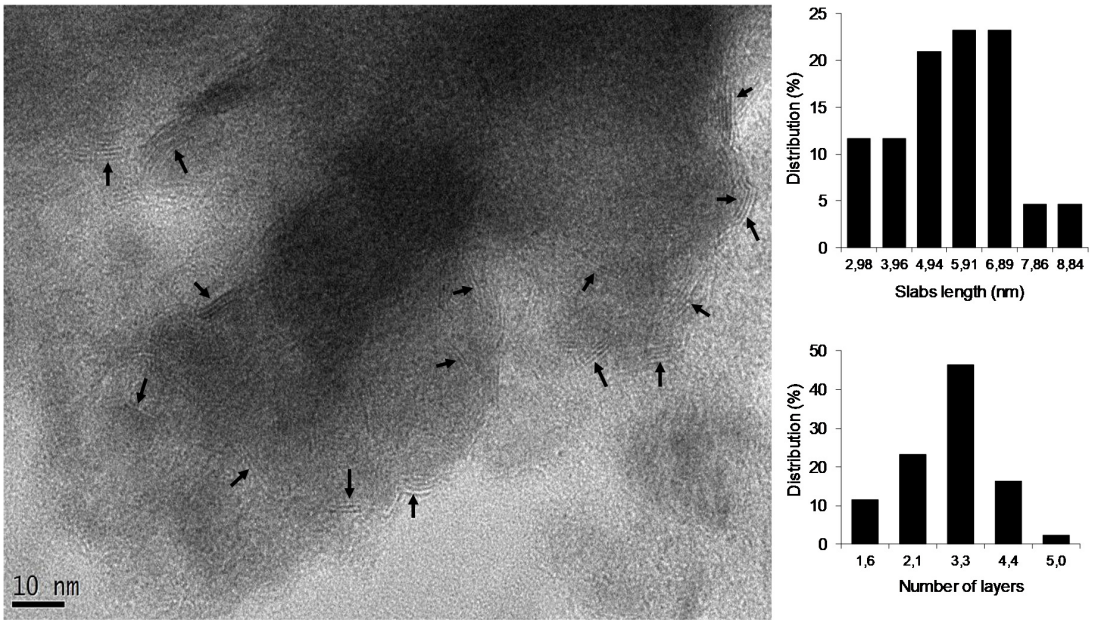

Figure 6. HRTEM micrographs and distributions of slabs length and stacking degree in sulfided NiMoV-S/Al-Ga(1%-SG).

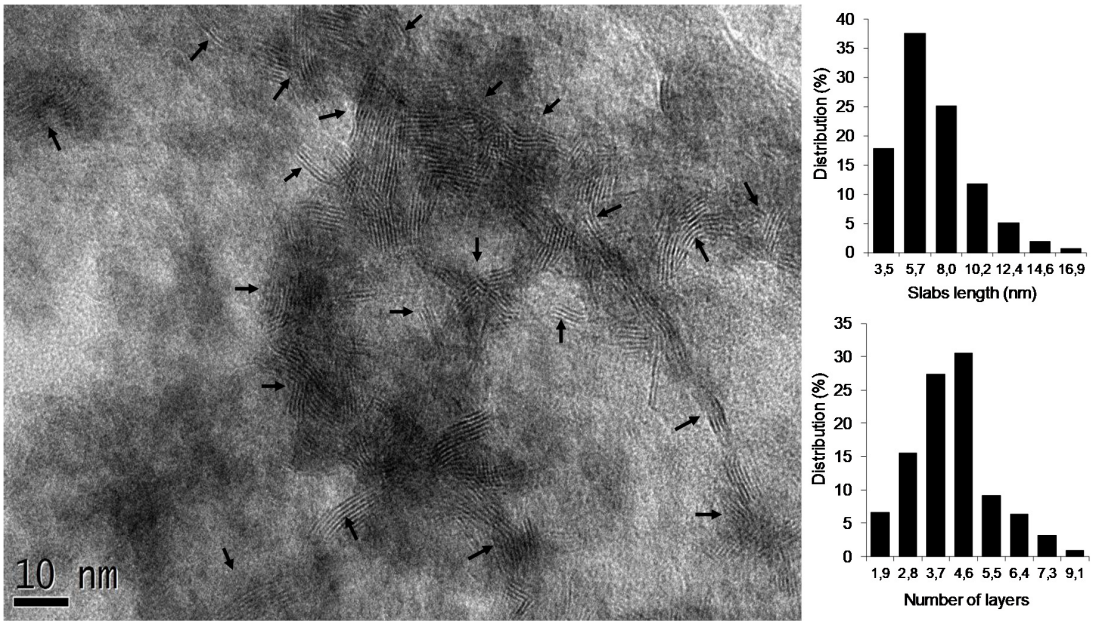

Figure 7. HRTEM micrographs and distributions of slabs length and stacking degree in sulfided NiMoV-S/Al-Ga(1%-I).

2.7. Catalytic Test

The dibenzothiophene HDS activities in function of the product conversion of the NiMo-S/Al_2O_3, NiMoV-S/Al-Ga(1%-SG) and NiMoV-S/Al-Ga(1%-I) catalysts are reported as overall pseudo-first-order rate constants after 6 h of reaction time. Hence, the main reaction products in the HDS of DBT were biphenyl (BP, direct desulfurization route), cyclohexylbenzene (CHB, hydrogenation route) and tetrahydrodibenzothiophene (THDBT), this latter being detected in appreciable amounts at low DBT HDS conversions (<70%) as shows the Figure 8 in the product distributions during reaction times. The catalysts obtained show a large effect of the support synthesis method on intrinsic HDS activities, since the overall activities were found to increase as follows: NiMoV-S/Al-Ga(1%-I) < NiMo-S/Al_2O_3

< NiMoV-S/Al-Ga(1%-SG), i.e., overall pseudo-first-order rate constants' values (k) of 1.65, 2.47 and 7.07 L/(h·mol·m^2), respectively. Likewise, all HDS lead to higher DDS activity (BP formation) with conversions of 85, 87 and 90% for NiMoV-S/Al-Ga(1%-SG), NiMo-S/Al_2O_3 and NiMoV-S/Al-Ga(1%-I), respectively (see Table 3). The hydrogenation abilities of the catalysts in the HDS reaction was calculated with the HYD/DDS ratios: NiMoV-S/Al-Ga(1%-SG) < NiMo-S/Al_2O_3 < NiMoV-S/Al-Ga(1%-I). Thus, the introduction of Ga and V to NiMoV-S/Al-Ga(1%-SG) resulted in almost a three-fold increase of the rate constant than their unpromoted analog, while NiMoV-S/Al-Ga(1%-I) was more than half; display that NiMoV-S/Al-Ga(1%-SG) was the most active between the synthesized and tested catalysts. This result suggests that the way to incorporate Ga into the support influences the dispersion of the V^{5+} species (structural promoter) [30]. It is well known that Ga-incorporation into A_2O_3-framework provides an increased number of acid sites that allow a better dispersion [20]. In the case of NiMoV-S/Al-Ga(1%-I) was observed small V rich-aggregates with greater presence of Ga on the surface that favors good hydrogenating properties NiMoS [20,21].

Table 3. Apparent rate constants of NiMoV-S/Al-Ga(1%-x) catalyst varying the synthesis method (x = SG and I) for DBT hydrodesulfurization (HDS) and naphthalene hydrogenation (HYD) in the reaction network shown in Schemes 1 and 2.

Catalysts	HDS Rate Constants, L/(h·mol·m^2)					HYD Rate Constants, L/(h·mol·m^2)			
	K_{HDS}	k_1*	k_2*	k_3* (×10^{-10})	k_4*	HYD/DDS	k_1*	k_2*	k_3*
NiMo-S/Al_2O_3	2.47	2.15	0.314	5.62	46.2	0.15	0.454	0.151	0.164
NiMoV-S/Al-Ga(1%-SG)	7.07	6.34	0.732	0.112	79.1	0.12	0.481	0.022	0.057
NiMoV-S/Al-Ga(1%-I)	1.65	1.40	0.254	0.019	24.5	0.18	1.02	1.61	2.23

kn*, apparent rate constant.

The aforementioned can be confirmed with naphthalene HYD activities, which shows that NiMoV-S/Al-Ga(1%-I) was more active than NiMo-S/Al_2O_3 and NiMoV-S/Al-Ga(1%-SG) with conversions around 35% as shown in Figure 8. It showed a higher rate of constants' values (k), which varied in a wide range, from 0.022 to 2.23 L/(h·mol·m^2) (see Table 3). Liu et al. reported in their studies of naphthalene HYD on highly-loaded NiMo catalysts that the morphological differences of the agglomerated active components (MoS_2 nanoparticles) can be the main reason of their hydrogenation ability and in this sense our NiMoV-S/Al-Ga(1%-I) exhibited much larger MoS_2 nanoparticles than NiMoV-S/Al-Ga(1%-SG) as revealed by HRTEM analysis, suggesting that the hydrogenated intermediate tetralin did not need to desorb from the catalyst surface since there might exist enough space for the total hydrogenation reactions; whereas NiMo-S/Al_2O_3 and NiMoV-S/Al-Ga(1%-SG) showed a higher selectivity towards tetralin, probably due to a function of adsorption nature more than hydrogenation ability of the catalyst [47]. Resuming all the above observations, we consider that Ga and V act as structural promoters in the NiMo catalysts supported on Al_2O_3 that allows the largest generation of BRIM sites for HYD and coordinative unsaturated sites (CUS) for DDS.

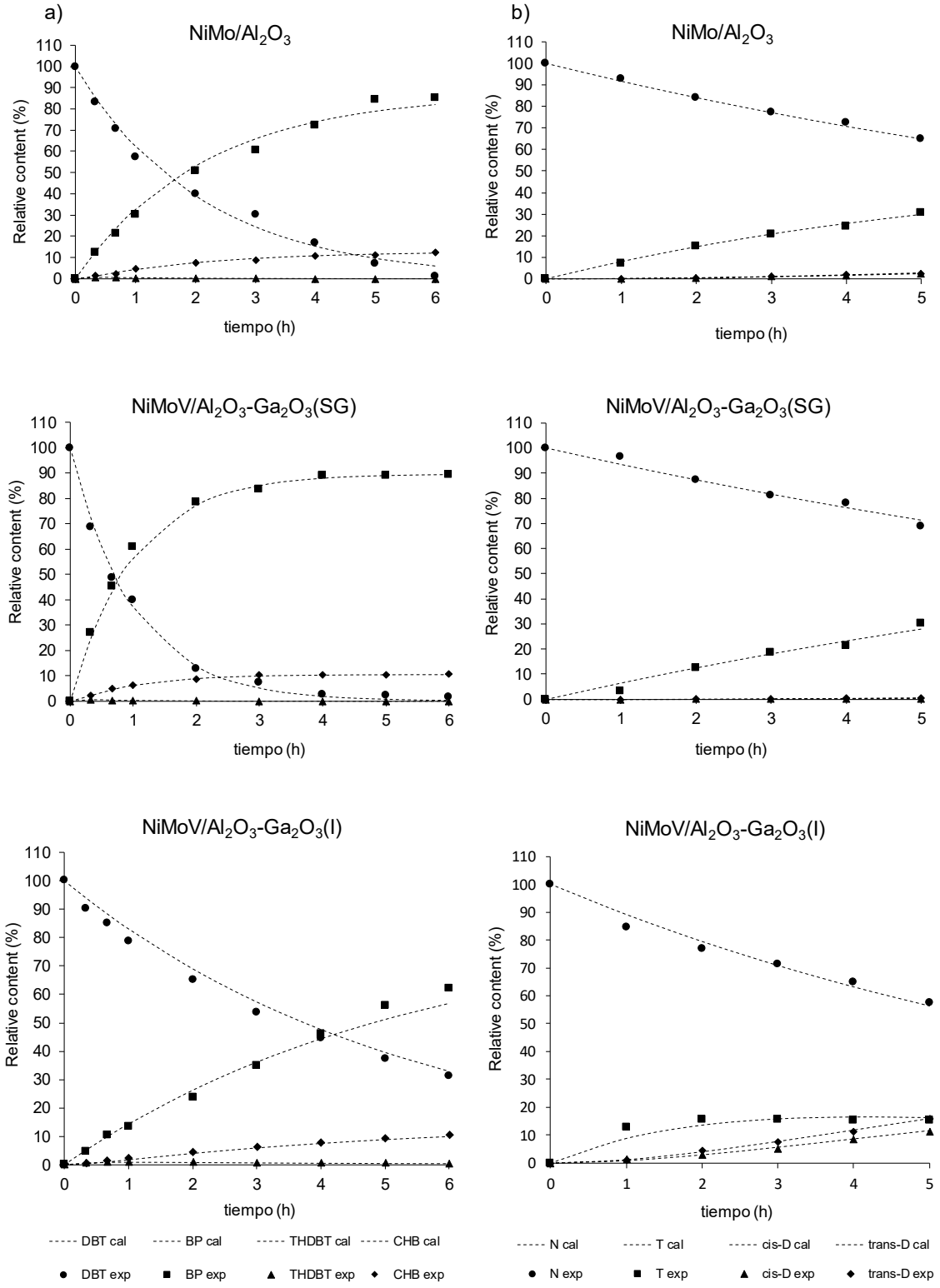

Figure 8. Reaction reactant and products compositions of NiMoV-S/Al-Ga(1%-x) varying the synthesis method (x = SG and I). (**a**) Dibenzothiophene HDS and (**b**) naphthalene HYD. The fitted curves were based on the Equations (3)–(10) of Schemes 1 and 2.

3. Materials and Methods

3.1. Preparation of Alumina Modified with Gallium

The catalytic supports with 1 wt% as Ga_2O_3 was prepared by two different methods that will be identified as Al_2O_3-Ga_2O_3(1%-SG) and Ga_2O_3/Al_2O_3(1%-I). Al_2O_3-Ga_2O_3(1%-SG) was prepared by the one-pot sol-gel synthesis [34]. In a typical experiment, appropriate amounts of aluminum(III)isopropylate ($Al[OCH(CH_3)_2]_3$, 99.8%, Sigma-Aldrich), and gallium(III)acetylacetonate ($Ga[CH_3COCH=C(O-)CH_3]_3$, 99.9%, Sigma-Aldrich) were dispersed in 50 mL of isopropanol ($(CH_3)_2CHOH$, 98%, Sigma-Aldrich) under magnetic stirring at about 75–77 °C until obtaining a homogeneous solution. Subsequently, the polymerized solution of $Al[OCH(CH_3)_2]_3$/ $Ga[CH_3COCH=C(O-)CH_3]_3$ was slowly added to a surfactants solution obtained homogenizing 56.5 mmol of tetramethylammonium hydroxide (TMAOH, 25% in H_2O, Sigma-Aldrich) and 18.1 mmol of hexadecyltrimethylammonium bromide (CTMAB, 99 %, Sigma-Aldrich) in 30 mL of deionized water. After that, the pH was adjusted at 8–10 with diluted ammonium hydroxide (NH_4OH, 28.0–30.0% NH_3 basis, Sigma-Aldrich), keeping under stirred for 2 h. The resulting mixture was aged for 48 h without stirring, filtered, washed, dried at 393 K for 12 h, pulverized and calcined at 883 K for 6 h.

In the other hand, The Ga_2O_3/Al_2O_3(1%-I) was prepared by impregnation over pore volume adding dropwise to a flask containing 5 g of Al_2O_3 (alumina was obtained as above-mentioned without adding gallium) an aqueous solution of $Ga[CH_3COCH=C(O-)CH_3]_3$ at 353 K, under stirring and pH 6. after removing the solvent by evaporation, the as-made sample was dried at 383 K for 12 h and then it was calcined at 883 K for 6 h.

3.2. Preparation of Catalyst Precursors Supported on Modified Alumina with Gallium

The vanadium was impregnated on 3 g of Al_2O_3-Ga_2O_3(1%-I) and Al_2O_3-Ga_2O_3(1%-SG) over pore volume adding dropwise an acidified aqueous solution of ammonium metavanadate (5.5 wt% V_2O_5, sigma-Aldrich 98%) at 353 K, under stirring and pH 5–6 until that the solvent is removed by evaporation. The mass obtained was dried at 383 K for 12 h and then it was calcined at 773 K for 4 h. Later, three types of catalytic precursors to 20 wt% Mo were synthesized impregnating in excess of pore volume 3 g of V_2O_5/Al_2O_3-Ga_2O_3(1%-I), V_2O_5/Al_2O_3-Ga_2O_3(1%-SG) and Al_2O_3 with an aqueous solution of Anderson ammonium salt ($(NH_4)_4[NiMo_6O_{24}H_6]\bullet 5H_2O$) under stirring at 323 K and pH around 5–6, respectively. The impregnation step lasted until the removal of the solvent by evaporation and the mass obtained was further dried at 378 K for 12 h [31].

The $(NH_4)_4[NiMo_6O_{24}H_6]\bullet 5H_2O$ supported on alumina modified with gallium and vanadium will be identified as NiMoV/Al-Ga(1%-x), where x is the synthesis method of the support (SG: sol-gel and I: impregnation). Likewise, NiMoV/Al-Ga(1%-x) sulfided will be identified as NiMoV-S/Al-Ga(1%-x).

3.3. Catalyst Characterization

The elemental analysis for NiMoV/Al-Ga(1%-x) was determined by XRF using a MagixPro PW–2440 Philips instrument. Sulfur elemental analysis was carried out employing a combustion method employing a Fisons EA 1108 CHNS-O analyzer in solids HDS postreaction. The textural properties were determined utilizing the physisorption technique of N_2 at 77 K using a Micromeritics 3FLEXTM instrument. The surface areas of samples were calculated by the Brunauer–Emmett–Teller multipoint method (BET) and, total pore volume and pore size distribution were determined from the adsorption branch of the isotherm using the Barret–Joyner–Halenda (BJH) model [48]. XRD analysis of the samples was carried out using a BRUKER D8 ADVANCE diffractometer with a Cu Kα radiation source (λ = 1.5418 Å) and Ni filter, within the range $5° \leq 2\theta \leq 90°$, step size of 0.02° and acquisition speed of 0.08°/s. Identification of the different phases was made using the JCPDS library [37]. The surface composition of the sulfided catalysts was determined through of X-ray photoelectron spectroscopy (XPS) with a Thermo Scientific K-Alpha spectrometer, equipped with a dual (non-monochromatic) Mg/Al anode, operated at 400 W and under a vacuum better than 10^{-9} torr. Calibration of the instrument was carried out employing the Au $4f_{7/2}$ line at 83.9 eV. The internal referencing of binding

energies was made using the dominating Al 2p band of the support at 74,4 eV [49]. Morphology of the samples was observed by scanning electron microscopy (SEM) using a field emission scanning electron microscope (JEOL, model JSM-7800F, Japan) operated at 1 kV. The mapping images and elemental analysis characterization were acquired simultaneously at 15 kV using the energy-dispersive X-ray spectroscopy (EDS) analyzer coupled to the same JEOL 7800F instrument. The average morphology of the MoS_2 active phase in the catalysts was observed in HRTEM images, which were obtained on a JEOL 2010 microscope with a 1.9 Å point-to-point resolution at 200 kV. From 10 to 15 representative micrographs were obtained for each catalyst in high-resolution mode. Typically, the slabs lengths and stacking of least 350-400 crystallites of MoS_2 were measured for each catalyst along with its dispersion, the average fraction of Mo atoms at the MoS_2 edge surface was calculated as suggesting Li et al. [46].

3.4. Catalytic Test

Before the HDS and HYD catalytic reactions, 1.0 g of NiMoV/Al-Ga(1%-x) or $NiMo/Al_2O_3$ precursor were sulfiding ex-situ passing through them a total flow rate of 0.33 cm^3 min^{-1} CS_2(2 vol%)/heptane and 70 cm^3 min^{-1} of hydrogen at 623 K for 4 h to attain a reproducible and stable state at the surface [36]. The HDS and HYD test conditions were as follows: The dibenzothiophene/hexadecane (80 mL, 500 ppm of S) and naphthalene/hexadecane (80 mL, 0.12 M) solutions were introduced, respectively, into the autoclave (JP Inglobal) with 300 mg of catalyst and then the reactor was purged for three times by N_2 at ambient temperature and thereafter pressured to 3.1 MPa H_2. The mixture was heated from room temperature to 593 K for 6 h under constant stirring, then the dibenzothiophene and naphthalene consumption and products formed during the course of reaction were followed employing a CG-2014-Shimadzu equipped with a flame ionization detector (FID) and 30 m length *BP5* capillary column using standards of dibenzothiophene (DBT, Sigma-Aldrich 99%), biphenyl (BP, Sigma-Aldrich ≥ 99%), cyclohexylbenzene (CHB, Sigma-Aldrich ≥ 97%), tetrahydrodibenzothiophene (THDBT, GC-MS), naphthalene (N, Sigma-Aldrich 99%), tetralin (T, Sigma-Aldrich 99%), trans-decalin (trans-D, Sigma-Aldrich 99%), cis-decalin (cis-D, Sigma-Aldrich 99%). The effluents sampling of the reactor occurring at 0, 30, 60, 120, 180, 240, 300 and 360 min.

In the reaction both the alumina supporting, and the V or Ga-modified alumina showed negligible dibenzothiophene and naphthalene conversion. Absence of mass and heat flow transport effects was verified according to established procedures [50,51]. All experiments reported in this work (synthesis protocols, characterizations and catalytic activity measurements) were carried out at least in triplicate. Good reproducibility was verified, better than 10% in all quantitative measurements.

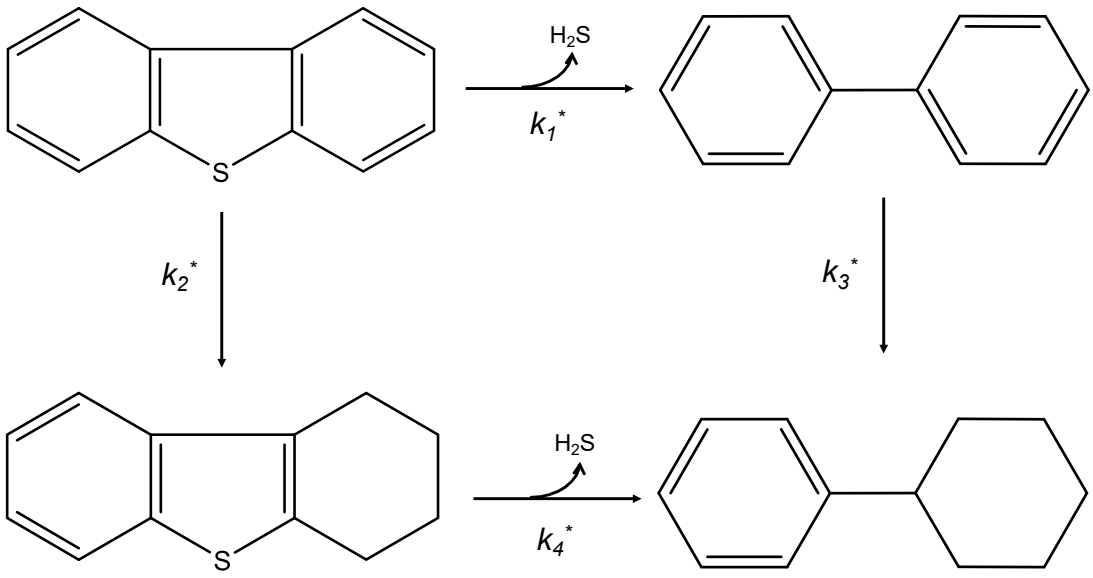

Scheme 1. Semi-empirical kinetic models of HDS [52].

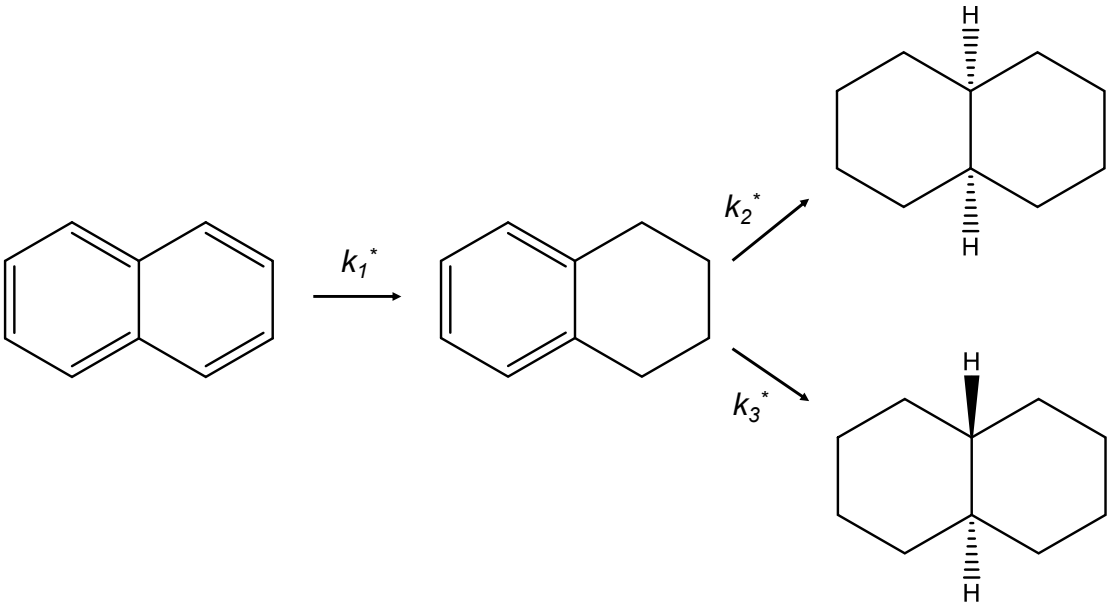

Scheme 2. Semi-empirical kinetic models of HYD [52].

The semi-empirical kinetic models of HDS and HYD were calculated according to the mechanism presented in the Schemes 1 and 2 [52,53], respectively. All the reactions were assumed irreversible due to the excess of hydrogen (considered constant), whereby the reactions are considered of the pseudo-first-order. The HDS kinetic model assumes the existence of active sites for hydrogenation and direct desulfurization, which can be expressed as $R_{Total} = R_{HYD} + R_{DDS}$, namely the overall pseudo-first order rate constant (k) as $k = k_1^* + k_2^*$, where k_1^* and k_2^* are the apparent rate constants for the DDS and HYD routes; while the naphthalene is firstly hydrogenated to tetralin, and later to decalin isomers as final reaction products.

The system of differential equations to calculate the catalytic constants was solved using the Maxima software and the nonlinear parameter estimations were calculated until converged by minimizing the deviation from experimental concentrations using the Levenberg–Marquardt algorithm of the Origin 9 version. In this approach, the apparent rate constants of the dibenzothiophene HDS and naphthalene HYD were calculated as k_1^*, k_2^*, k_3^* and k_4^* (Equations (1)–(4)) and k_1^*, k_2^* and k_3^* (Equations (5)–(8)), which are defined by $kn^* = knKn$, where kn and Kn are the intrinsic rate and the equilibrium adsorption constants, respectively.

$$C_{DBT} = C_{DBT_0} \cdot e^{-kt} \tag{1}$$

$$C_{BP} = \frac{C_{DBT_0} \cdot k_{1*}}{k_{3*} - k}\left[e^{-kt} - e^{-k_{3*}t}\right] \tag{2}$$

$$C_{THDBT} = \frac{C_{DBT_0} \cdot k_{2*}}{k_{4*} - k}\left[e^{-kt} - e^{-k_4*t}\right] \tag{3}$$

$$C_{CHB} = \frac{C_{DBT_0} \cdot k_{3*} \cdot k_{1*}}{k_{3*} - k}\left[\frac{1}{k_{3*}}e^{-k_{3*}t} - \frac{1}{k}e^{-kt}\right] + \frac{C_{DBT_0} \cdot k_{4*} \cdot k_{2*}}{k_{4*} - k}\left[\frac{1}{k_{4*}}e^{-k_{4*}t} - \frac{1}{k}e^{-kt}\right] + \frac{C_{DBT_0}(k_{1*} + k_{2*})}{k} \tag{4}$$

$$C_N = C_{N_0} \cdot e^{-k_1*t} \tag{5}$$

$$C_T = \frac{C_{N_0} \cdot k_{1*}}{(k_{2*} + k_{3*}) - k_{1*}}\left[e^{-k_{1*}t} - e^{-(k_{2*} + k_{3*})t}\right] \tag{6}$$

$$C_{cisD} = C_{N_0}\left[\frac{k_{2*}}{(k_{2*}+k_{3*})} - \frac{k_{1*}\cdot k_{2*}}{(k_{2*}+k_{3*})\cdot(k_{1*}-k_{2*}-k_{3*})}e^{-(k_{2*}+k_{3*})t} + \frac{k_{2*}}{k_{1*}-k_{2*}-k_{3*}}e^{-k_{1*}t}\right] \quad (7)$$

$$C_{transD} = C_{N_0}\left[\frac{k_{3*}}{(k_{2*}+k_{3*})} - \frac{k_{1*}\cdot k_{3*}}{(k_{2*}+k_{3*})\cdot(k_{1*}-k_{2*}-k_{3*})}e^{-(k_{2*}+k_{3*})t} + \frac{k_{3*}}{k_{1*}-k_{2*}-k_{3*}}e^{-k_{1*}t}\right] \quad (8)$$

Finally, the HDS and HYD activities of the catalysts are reported as pseudo-first-order rate constant for dibenzothiophene and naphthalene disappearance normalized by the concentration (mol/L) of DBT or N per weight (m_{cat}, g) and surface area (S_{BET}, m^2/g) of the catalyst after ~ 5–6 h of reaction time.

4. Conclusions

In the present work, two NiMoV catalysts supported on Al_2O_3-Ga_2O_3(1%-x) were prepared using two synthesis method different. The changes in the support's composition with gallium and vanadium as promoter resulted in properties different and dispersion of the MoS_2 particles. The evaluation of the NiMoV/Al_2O_3-Ga_2O_3(1%-x) catalysts in the DBT hydrodesulfurization and NP hydrogenation showed that the catalysts presented significant differences in the activity and selectivity of the products. In this respect, the chemical analyses by FRX for the NiMoV/Al_2O_3-Ga_2O_3(x) catalysts showed stoichiometric values Mo/Ni ~ 6 and (V + Ni)/(V + Ni + Mo)= 0.31–0.34, while EDS spectra and elemental mapping confirmed the presence of Ni, Mo, V, Ga, S, Al and O with well-distribution on support. The NiMo/Al_2O_3 and NiMoV/Al_2O_3-Ga_2O_3(1%-SG) showed better textural properties than NiMoV/Al_2O_3-Ga_2O_3(1%-I) with average pore radius between 6.18 and 7.89 nm. XRD confirmed the presence of $(NH_4)_4[NiMo_6O_{24}H_6]\bullet 5H_2O$ and XPS evidenced Mo^{4+}, Mo^{6+}, Ni_xS_y, Ni^{2+}, Ga^{3+} and V^{5+} species, which shown a dependence with the synthesis method of the support, whereas gallium and vanadium oxides were not detected due to the well dispersed on the support, suggesting that the synthesis method via impregnation induced largest presence of gallium on the surface allowing a better dispersion of V^{5+} oxides influencing in the degree of sulfidation. The HRTEM analysis shown that the length and stacking distribution of MoS_2 crystallites changes with the support synthesis method varied from 5.07 to 5.94 nm and 2.74 to 3.58, respectively. The activities as dibenzothiophene HDS overall pseudo-first-order rate constants' values (k_{HDS}) from 1.65 to 7.07 L/(h·mol·m^2), and naphthalene HYD activity with rate constants' values (k) from 0.022 to 2.23 L/(h·mol·m^2). The previous observations allow us to conclude that Ga and V act as structural promoters in the NiMo catalysts supported on Al_2O_3 that contribute in the largest generation of BRIM sites for HYD and CUS sites for DDS.

Author Contributions: Conceptualization, E.P.-P. and E.M.; methodology, E.P.-P.; software, E.P.-P.; validation, E.P.-P., E.M., and Y.P.; formal analysis, Y.P.; investigation, E.P.-P.; resources, Y.P.; data curation, E.P.-P. and E.M.; writing—original draft preparation, E.M.; writing—review and editing, E.P.-P., E.M., and Y.P.; visualization, E.M.; supervision, E.P.-P., E.M., and Y.P.; project administration, E.P.-P. and E.M.; funding acquisition, E.P.-P.; resources, E.P.-P., E.M. and Y.P.. All authors have read and agreed to the published version of the manuscript.

Funding: This research received no external funding.

Acknowledgments: The authors also gratefully the financial support provided by Universidad del Norte, under Project number: 2019-017. Besides, The authors would like to acknowledge financial support to Universidad del Atlántico (through equidad investigativa y "1º convocatoria interna para apoyo al Desarrollo de trabajos de grado en investigación formativa nivel pregrado y postgrado").

Conflicts of Interest: The authors declare no conflict of interests.

References

1. Anderson, J.R.; Boudart, M. *Catalysis: Science and Technology*; Springer: Berlin/Heidelberg, Germany, 1996; ISBN 978-3-642-61040-0.
2. Rașeev, S.D. *Thermal and Catalytic Processes in Petroleum Refining*; Marcel Dekker: New York, NY, USA, 2003; ISBN 978-0-8247-0952-5.

3. Lødeng, R.; Hannevold, L.; Bergem, H.; Stöcker, M. Catalytic Hydrotreatment of Bio-Oils for High-Quality Fuel Production. In *The Role of Catalysis for the Sustainable Production of Bio-Fuels and Bio-Chemicals*; Triantafyllidis, K.S., Lappas, A.A., Stöcker, M., Eds.; Elsevier: Amsterdam, The Netherlands, 2013; Chapter 11; pp. 351–396. ISBN 978-0-444-56330-9.
4. Debecker, D.P.; Stoyanova, M.; Rodemerck, U.; Gaigneaux, E.M. Preparation of MoO_3/SiO_2–Al_2O_3 metathesis catalysts via wet impregnation with different Mo precursors. *J. Mol. Catal. Chem.* **2011**, *340*, 65–76. [CrossRef]
5. Topsøe, H.; Clausen, B.S. Active sites and support effects in hydrodesulfurization catalysts. *Appl. Catal.* **1986**, *25*, 273–293. [CrossRef]
6. Chianelli, R.R.; Siadati, M.H.; De la Rosa, M.P.; Berhault, G.; Wilcoxon, J.P.; Bearden, R.; Abrams, B.L. Catalytic Properties of Single Layers of Transition Metal Sulfide Catalytic Materials. *Catal. Rev.* **2006**, *48*, 1–41. [CrossRef]
7. Babich, I. Science and technology of novel processes for deep desulfurization of oil refinery streams: A review. *Fuel* **2003**, *82*, 607–631. [CrossRef]
8. Ministerio de Ambiente y Desarrollo Sostenible, y Ministerio de Minas y Energías. *Resolución 40619* **2017** pág 1-3; *Resolución 90963* **2014**, 5.
9. Gutiérrez, O.Y.; Klimova, T. Effect of the support on the high activity of the (Ni)Mo/ZrO_2–SBA-15 catalyst in the simultaneous hydrodesulfurization of DBT and 4,6-DMDBT. *J. Catal.* **2011**, *281*, 50–62. [CrossRef]
10. Rashidi, F.; Sasaki, T.; Rashidi, A.M.; Nemati Kharat, A.; Jozani, K.J. Ultradeep hydrodesulfurization of diesel fuels using highly efficient nanoalumina-supported catalysts: Impact of support, phosphorus, and/or boron on the structure and catalytic activity. *J. Catal.* **2013**, *299*, 321–335. [CrossRef]
11. Chianelli, R.R. Fundamental Studies of Transition Metal Sulfide Hydrodesulfurization Catalysts. *Catal. Rev.* **1984**, *26*, 361–393. [CrossRef]
12. Topsøe, H.; Clausen, B.S.; Massoth, F.E. Hydrotreating Catalysis. In *Catalysis*; Anderson, J.R., Boudart, M., Eds.; Springer: Berlin/Heidelberg, Germany, 1996; pp. 1–269. ISBN 978-3-642-64666-9.
13. Breysse, M.; Portefaix, J.L.; Vrinat, M. Support effects on hydrotreating catalysts. *Catal. Today* **1991**, *10*, 489–505. [CrossRef]
14. Palcheva, R.; Kaluža, L.; Spojakina, A.; Jirátová, K.; Tyuliev, G. NiMo/γ-Al_2O_3 Catalysts from Ni Heteropolyoxomolybdate and Effect of Alumina Modification by B, Co, or Ni. *Chin. J. Catal.* **2012**, *33*, 952–961. [CrossRef]
15. Jirátová, K.; Kraus, M. Effect of support properties on the catalytic activity of HDS catalysts. *Appl. Catal.* **1986**, *27*, 21–29. [CrossRef]
16. Saini, A.R.; Johnson, B.G.; Massoth, F.E. Studies of molybdena—Alumina catalysts XIV. Effect of Cation-Modified Aluminas. *Appl. Catal.* **1988**, *40*, 157–172. [CrossRef]
17. Strohmeier, B. Surface spectroscopic characterization of the interaction between zinc ions and $gamma;-alumina. *J. Catal.* **1984**, *86*, 266–279. [CrossRef]
18. Cabello, C.I.; Botto, I.L.; Thomas, H.J. Anderson type heteropolyoxomolybdates in catalysis:: 1. (NH4)3[CoMo6O24H6]·7H2O/γ-Al2O3 as alternative of Co-Mo/γ-Al2O3 hydrotreating catalysts. *Appl. Catal. Gen.* **2000**, *197*, 79–86. [CrossRef]
19. Cabello, C.I.; Cabrerizo, F.M.; Alvarez, A.; Thomas, H.J. Decamolybdodicobaltate(III) heteropolyanion: Structural, spectroscopical, thermal and hydrotreating catalytic properties. *J. Mol. Catal. Chem.* **2002**, *186*, 89–100. [CrossRef]
20. Altamirano, E.; de los Reyes, J.A.; Murrieta, F.; Vrinat, M. Hydrodesulfurization of 4,6-dimethyldibenzothiophene over Co(Ni)MoS2 catalysts supported on alumina: Effect of gallium as an additive. *Catal. Today* **2008**, *133–135*, 292–298. [CrossRef]
21. Díaz de León, J.N.; Picquart, M.; Massin, L.; Vrinat, M.; de los Reyes, J.A. Hydrodesulfurization of sulfur refractory compounds: Effect of gallium as an additive in NiWS/γ-Al_2O_3 catalysts. *J. Mol. Catal. Chem.* **2012**, *363–364*, 311–321. [CrossRef]
22. Cimino, A.; Lo Jacono, M.; Schiavello, M. Effect of zinc, gallium, and germanium ions on the structural and magnetic properties of nickel ions supported on alumina. *J. Phys. Chem.* **1975**, *79*, 243–249. [CrossRef]
23. Zepeda, T.A.; Pawelec, B.; Díaz de León, J.N.; de los Reyes, J.A.; Olivas, A. Effect of gallium loading on the hydrodesulfurization activity of unsupported Ga2S3/WS2 catalysts. *Appl. Catal. B Environ.* **2012**, *111–112*, 10–19. [CrossRef]

24. Petre, A.L.; Auroux, A.; Gervasini, A.; Caldararu, M.; Ionescu, N.I. Calorimetric Characterization of Surface Reactivity of Supported Ga_2O_3 Catalysts. *J. Therm. Anal. Calorim.* **2001**, *64*, 253–260. [CrossRef]
25. Dejonghe, S.; Hubaut, R.; Grimblot, J.; Bonnelle, J.P.; Des Courieres, T.; Faure, D. Hydrodemetallation of a vanadylporphyrin over sulfided NiMoγAl_2O_3, MoγAl_2O_3, and γAl_2O_3 catalysts—Effect of the vanadium deposit on the toluene hydrogenation. *Catal. Today* **1990**, *7*, 569–585. [CrossRef]
26. Rankel, L.; Rollmann, L. Catalytic activity of metals in petroleum and their removal. *Fuel* **1983**, *62*, 44–46. [CrossRef]
27. Lacroix, M.; Boutarfa, N.; Guillard, C.; Vrinat, M.; Breysse, M. Hydrogenating properties of unsupported transition metal sulphides. *J. Catal.* **1989**, *120*, 473–477. [CrossRef]
28. Betancourt, P.; Rives, A.; Scott, C.E.; Hubaut, R. Hydrotreating on mixed vanadium–nickel sulphides. *Catal. Today* **2000**, *57*, 201–207. [CrossRef]
29. Betancourt, P.; Marrero, S.; Pinto-Castilla, S. V–Ni–Mo sulfide supported on Al_2O_3: Preparation, characterization and LCO hydrotreating. *Fuel Process. Technol.* **2013**, *114*, 21–25. [CrossRef]
30. Escalante, Y.; Méndez, F.J.; Díaz, Y.; Inojosa, M.; Morgado, M.; Delgado, M.; Bastardo-González, E.; Brito, J.L. MCM-41-supported vanadium catalysts structurally modified with Al or Zr for thiophene hydrodesulfurization. *Appl. Petrochem. Res.* **2019**, *9*, 47–55. [CrossRef]
31. Ayala-G, M.; Puello, E.; Quintana, P.; González-García, G.; Diaz, C. Comparison between alumina supported catalytic precursors and their application in thiophene hydrodesulfurization: $(NH_4)[NiMo_6O_{24}H_6]\cdot 5H_2O/\gamma$-$Al_2O_3$ and NiMoOx/γ-Al_2O_3 conventional systems. *RSC Adv.* **2015**, *5*, 102652–102662. [CrossRef]
32. Thommes, M.; Kaneko, K.; Neimark, A.V.; Olivier, J.P.; Rodriguez-Reinoso, F.; Rouquerol, J.; Sing, K.S.W. Physisorption of gases, with special reference to the evaluation of surface area and pore size distribution (IUPAC Technical Report). *Pure Appl. Chem.* **2015**, *87*, 1051–1069. [CrossRef]
33. Sampieri, A.; Pronier, S.; Brunet, S.; Carrier, X.; Louis, C.; Blanchard, J.; Fajerwerg, K.; Breysse, M. Formation of heteropolymolybdates during the preparation of Mo and NiMo HDS catalysts supported on SBA-15: Influence on the dispersion of the active phase and on the HDS activity. *Microporous Mesoporous Mater.* **2010**, *130*, 130–141. [CrossRef]
34. Haneda, M.; Kintaichi, Y.; Shimada, H.; Hamada, H. Selective Reduction of NO with Propene over Ga_2O_3–Al2O3: Effect of Sol–Gel Method on the Catalytic Performance. *J. Catal.* **2000**, *192*, 137–148. [CrossRef]
35. Ueno, A.; Suzuki, H.; Kotera, Y. Particle-size distribution of nickel dispersed on silica and its effects on hydrogenation of propionaldehyde. *J. Chem. Soc. Faraday Trans. 1 Phys. Chem. Condens Phases* **1983**, *79*, 127. [CrossRef]
36. Puello-Polo, E.; Marquez, E.; Brito, J.L. One-pot synthesis of Nb-modified Al_2O_3 support for NiMo hydrodesulfurization catalysts. *J. Sol-Gel Sci. Technol.* **2018**, *88*, 90–99. [CrossRef]
37. International Centre for Diffraction Data®(ICDD®). *Power Diffraction File*; ICDD: Newtown Square, PA, USA, 1995.
38. Galtayries, A.; Wisniewski, S.; Grimblot, J. Formation of thin oxide and sulphide films on polycrystalline molybdenum foils: Characterization by XPS and surface potential variations. *J. Electron Spectrosc. Relat. Phenom.* **1997**, *87*, 31–44. [CrossRef]
39. Weber, T.; Muijsers, J.C.; van Wolput, J.H.M.C.; Verhagen, C.P.J.; Niemantsverdriet, J.W. Basic Reaction Steps in the Sulfidation of Crystalline MoO_3 to MoS_2, As Studied by X-ray Photoelectron and Infrared Emission Spectroscopy. *J. Phys. Chem.* **1996**, *100*, 14144–14150. [CrossRef]
40. Aigler, J.M.; Brito, J.L.; Leach, P.A.; Houalla, M.; Proctor, A.; Cooper, N.J.; Hall, W.K.; Hercules, D.M. ESCA study of "model" allyl-based molybdenum/silica catalysts. *J. Phys. Chem.* **1993**, *97*, 5699–5702. [CrossRef]
41. Le, Z.; Afanasiev, P.; Li, D.; Long, X.; Vrinat, M. Solution synthesis of the unsupported Ni–W sulfide hydrotreating catalysts. *Catal. Today* **2008**, *130*, 24–31. [CrossRef]
42. Wang, X.; Ozkan, U.S. Characterization of Active Sites over Reduced Ni–Mo/Al_2O_3 Catalysts for Hydrogenation of Linear Aldehydes. *J. Phys. Chem. B* **2005**, *109*, 1882–1890. [CrossRef]
43. Schön, G. Auger and direct electron spectra in X-ray photoelectron studies of zinc, zinc oxide, gallium and gallium oxide. *J. Electron Spectrosc. Relat. Phenom.* **1973**, *2*, 75–86. [CrossRef]
44. Escaño, M.C.S.; Asubar, J.T.; Yatabe, Z.; David, M.Y.; Uenuma, M.; Tokuda, H.; Uraoka, Y.; Kuzuhara, M.; Tani, M. On the presence of Ga2O sub-oxide in high-pressure water vapor annealed AlGaN surface by combined XPS and first-principles methods. *Appl. Surf. Sci.* **2019**, *481*, 1120–1126. [CrossRef]

45. Rakmae, S.; Osakoo, N.; Pimsuta, M.; Deekamwong, K.; Keawkumay, C.; Butburee, T.; Faungnawakij, K.; Geantet, C.; Prayoonpokarach, S.; Wittayakun, J.; et al. Defining nickel phosphides supported on sodium mordenite for hydrodeoxygenation of palm oil. *Fuel Process. Technol.* **2020**, *198*, 106236. [CrossRef]
46. Li, M.; Li, H.; Jiang, F.; Chu, Y.; Nie, H. The relation between morphology of (Co)MoS_2 phases and selective hydrodesulfurization for CoMo catalysts. *Catal. Today* **2010**, *149*, 35–39. [CrossRef]
47. Liu, H.; Liu, C.; Yin, C.; Liu, B.; Li, X.; Li, Y.; Chai, Y.; Liu, Y. Low temperature catalytic hydrogenation naphthalene to decalin over highly-loaded NiMo, NiW and NiMoW catalysts. *Catal. Today* **2016**, *276*, 46–54. [CrossRef]
48. Barrett, E.P.; Joyner, L.G.; Halenda, P.P. The Determination of Pore Volume and Area Distributions in Porous Substances. I. Computations from Nitrogen Isotherms. *J. Am. Chem. Soc.* **1951**, *73*, 373–380. [CrossRef]
49. Farojr, A.; Dossantos, A. Cumene hydrocracking and thiophene HDS on niobia-supported Ni, Mo and Ni–Mo catalysts. *Catal. Today* **2006**, *118*, 402–409. [CrossRef]
50. Froment, G.F.; De Wilde, J.; Bischoff, K.B. *Chemical Reactor Analysis and Design*, 3rd ed.; Wiley: Hoboken, NJ, USA, 2011; ISBN 978-0-470-56541-4.
51. Moulijn, J.A.; Tarfaoui, A.; Kapteijn, F. General aspects of catalyst testing. *Catal. Today* **1991**, *11*, 1–12. [CrossRef]
52. Farag, H. Kinetic Analysis of the Hydrodesulfurization of Dibenzothiophene: Approach Solution to the Reaction Network. *Energy Fuels* **2006**, *20*, 1815–1821. [CrossRef]
53. Vargas-Villagrán, H.; Ramírez-Suárez, D.; Ramírez-Muñoz, G.; Calzada, L.A.; González-García, G.; Klimova, y.T.E. Tuning of activity and selectivity of Ni/(Al)SBA-15 catalysts in naphthalene hydrogenation. *Catal. Today* **2019**, S0920586119305103. [CrossRef]